Pergamon

Int. J. Heat Mass Transfer. Vol. 39, No. 16, pp. 3465–3474, 1996

0017-9310/96 $15.00+0.00

PII: S0017-9310(96)00007-5

A nonlinear low-Reynolds-number k–ε model for turbulent separated and reattaching flows—II. Thermal field computations

GWANG HOON RHEE and HYUNG JIN SUNG†

Department of Mechanical Engineering, Korea Advanced Institute of Science and Technology, 373-1, Kusong-dong, Yusong-ku, Taejon, 305-701, Korea

(*Received* 17 *February* 1995 *and in final form* 25 *October* 1995)

Abstract—As a sequence of the prior low-Reynolds-number k–ε model of Park and Sung, an improved version of the heat transfer model is developed for turbulent separated and reattaching flows. The equations of the temperature variance (k_θ) and its dissipation rate (ε_θ) are solved, together with the equations of k and ε. In the present model, the near-wall limiting behavior close to the wall and the nonequilibrium effect away from the wall are incorporated. The validation of the model is applied to the turbulent flow over a backward-facing step and the flow over a flat plate. The predictions of the present model are cross-checked with the existing measurements and DNS data. The model performance is shown to be generally satisfactory. Copyright © 1996 Elsevier Science Ltd.

1. INTRODUCTION

Separated and reattaching flows occur in many engineering problems. Examples may be found in nuclear reactors, gas turbines, electronic circuitry and heat transfer devises, to name a few. The flow separation and subsequent reattachment process generate extremely complex flow and heat transfer characteristics. Among others, they give rise to flow unsteadiness, pressure fluctuations, noise, etc. Also they tend to enhance heat and mass transfer and augment mixing. In particular, reattaching flows cause large variations of the local heat transfer coefficient, as well as substantial overall heat transfer augmentation. Thus, an accurate prediction of flow structure and attendant heat transport phenomena pose a significant and challenging task.

Comprehensive knowledge of flow structure is an essential building block to analyze the attendant heat transport phenomena. As a multi-prong attack on the problem of turbulent flow and heat transfer processes in separated and reattaching flows, an improved version of the nonlinear low-Reynolds-number k–ε model has been developed by Park and Sung [1]. In their model, the limiting near-wall behavior and nonlinear Reynolds stress representations were incorporated. The main emphasis was placed on the adoption of $R_y(\equiv k^{1/2}y/\nu)$ instead of $y^+(\equiv u_\tau y/\nu)$ in the low-Reynolds-number model, to avoid the difficulties at the separation and reattachment points ($u_\tau = 0$). The nonequilibrium effect was also taken into account to describe the recirculating flows away from the wall. The model performance was shown to be generally satisfactory. Based on the afore-mentioned fluid flow model, efforts are now directed toward extending the model to thermal field computation at the k–ε equation model level.

A literature survey reveals that most of studies on heat transfer in separated and reattaching flows have contained mainly mean heat transfer rates and very little fluid dynamic data [2–4]. However, in order to understand the dynamic characteristics of turbulent heat transfer, turbulence quantities are more informative. Contrary to the afore-said researches, studies on the combined heat transfer and fluid dynamic measurements in turbulent separated and reattaching flows are relatively scarce [5, 6]. Combined heat transfer and fluid dynamic measurements downstream of a backward-facing step have been made by Vogel and Eaton [5], in which the heat transfer data coupled with temperature and velocity profiles were provided to scrutinize the mechanisms of controlling the heat transfer rate in reattaching flows. Ota and Kon [6] presented heat transfer in the separated and reattaching flow over a blunt flat plate. By using the experimental data, they evaluated the eddy diffusivities of momentum (ν_t) and heat (α_t), as well as the turbulent Prandtl number ($Pr_t = \nu_t/\alpha_t$), in the thermal layer downstream of reattachment.

In contrast to the preceding rare experiments, there have been many numerical thermal field computations in turbulent separated and reattaching flows [7–10]. Most of the computations cited in the literature are implemented by using the k–ε model. Conventionally, the turbulent heat transfer is analyzed by employing the turbulent Prandtl number Pr_t, in which the eddy diffusivity for heat α_t is prescribed through the known

† Author to whom correspondence should be addressed.

NOMENCLATURE

c	specific heat
C_f	mean skin friction coefficient
C_μ, C_{ε_1}, C_{ε_2}	model constants of k–ε model
C_λ, $C_{\varepsilon_{\theta 1}}$, $C_{\varepsilon_{\theta 2}}$	model constants of k_θ–ε_θ model
f_μ, f_1, f_2, f_t	model functions of low-Reynolds-number k–ε model
$f_\lambda, f_{D_1}, f_{D_2}, f_h$	model functions of low-Reynolds-number k_θ–ε_θ model
H	height of backward-facing step
h	heat transfer coefficient $[=q_w/(T_w-T_\infty)]$
k	turbulent kinetic energy
k_θ	temperature variance
Pr	Prandtl number $(=\alpha/\nu)$
Pr_t	turbulent Prandtl number $(=\alpha_t/\nu_t)$
P_k	production of turbulent energy $(=-\overline{u_i u_j}\partial U_i/\partial x_j)$
P_θ	production of temperature variance $(=-\overline{u_i\theta}\partial T/\partial x_i)$
R	time scale ratio $(=t_\theta/t_v)$
R_t	turbulent Reynolds number $(=k^2/\nu\varepsilon)$
S_{ij}	strain rate tensor $[=0.5(U_{i,j}+U_{j,i})]$
St	Stanton number $(=h/U\rho c)$
T	mean temperature
t_v	turbulent time scale of flow field $(=k/\varepsilon)$
t_θ	turbulent time scale of thermal field $(=k_\theta/\varepsilon_\theta)$
X_R	reattachment length.

Greek symbols

α, α_t	thermal diffusivity and thermal eddy diffusivity
δ	boundary layer thickness
δ_θ	thermal boundary layer thickness
ε	dissipation rate of turbulent energy
ε_θ	dissipation rate of temperature variance
ν, ν_t	kinematic viscosity and eddy viscosity
ρ	density
σ_k, σ_ε	model constants in turbulent diffusion of k, ε equations
σ_{k_θ}, $\sigma_{\varepsilon_\theta}$	model constants in turbulent diffusion of k_θ, ε_θ equations
ω_{ij}	vorticity tensor $[=0.5(U_{i,j}-U_{j,i})]$.

eddy viscosity ν_t. This assumption, i.e. Pr_t = *constant*, satisfied Pope's linear principle of scalars in turbulent flows [11]. However, it is revealed that there are no universal values of Pr_t, even in simple attaching flows [12, 13]. Furthermore, it is expected that the values in separated and reattaching flows are substantially different from those in an ordinary boundary layer.

In order to analyze heat transfer problems numerically in separated and reattaching flows, a two-equation model for heat transport is more universal [14]. In this model, the eddy diffusivity for heat α_t is modeled by solving the two equations of temperature variance (k_θ) and its dissipation rates (ε_θ), together with k and ε. The modeling of the two-equation (k_θ–ε_θ) model has been attempted by many researchers [14–17]. Among others, Chung and Sung [15] have developed the four-equation turbulence model for an attached boundary layer, where the four equations imply the transport equations for k, ε, k_θ and ε_θ. Recently, a series of heat transfer two-equation models have been developed by Nagano's group [14, 16, 17]. Their models showed reasonable predictions of heat transfer in flows, with an almost complete dissimilarity between flow and thermal fields.

In the present study, an improved version of the low-Reynolds-number k_θ–ε_θ heat transfer model is proposed, in which the near-wall effect of separated and reattaching flows is fully incorporated. Emphasis is placed on the usage of R_y, instead of y^+ in the low-Reynolds-number model, together with the wall limiting behavior of the ε_θ equation. As a sequence of the prior model of Park and Sung [1], the thermal nonequilibrium effect ($P_\theta/\varepsilon_\theta$) is taken into account to deal with complex recirculation flows away from the wall. The model is tested with an attached boundary layer in the first. It is seen that the present model shows good prediction of DNS data in the near-wall region for both uniform wall temperature and uniform wall heat flux conditions [18, 19]. The model performance of the present model is then applied to the turbulent flow behind a backward-facing step and a blunt body with separation bubble. The predicted results of the present model are compared with the published experimental data [5, 6]. Furthermore, based on the computational results, the contour plots of Pr_t and $R(\equiv(k_\theta/\varepsilon_\theta)/k/\varepsilon))$ are visualized and analyzed.

2. TURBULENCE MODEL FOR VELOCITY FIELD

To evaluate accurately the turbulent heat transfer in separated and reattaching flows, the prediction of flow fields with sufficient accuracy should be preceded. As mentioned in the introduction, an improved version of the nonlinear low-Reynolds-number k–ε model for turbulent separated and reattaching flows has been developed by Park and Sung [1]. In this section, the model is briefly summarized. Details regarding the model formulations are compiled in Park and Sung.

For a stationary, incompressible flow field, the governing equations are in the following, with the equations of the turbulent kinetic energy k and its dissipation rate ε. These equations are written in Cartesian tensor notations as

$$\frac{\partial U_i}{\partial x_i} = 0 \tag{1}$$

$$U_j \frac{\partial U_i}{\partial x_j} = -\frac{\partial P}{\partial x_i} + \frac{\partial}{\partial x_j}\left[\nu \frac{\partial U_i}{\partial x_j} - \overline{u_i u_j}\right] \tag{2}$$

$$U_j \frac{\partial k}{\partial x_j} = \frac{\partial}{\partial x_j}\left[\left(\nu + f_t \frac{\nu_t}{\sigma_k}\right)\frac{\partial k}{\partial x_j}\right] + P_k - \varepsilon \tag{3}$$

$$U_j \frac{\partial \varepsilon}{\partial x_j} = \frac{\partial}{\partial x_j}\left[\left(\nu + f_t \frac{\nu_t}{\sigma_\varepsilon}\right)\frac{\partial \varepsilon}{\partial x_j}\right] + C^*_{\varepsilon_1} P_k \frac{\varepsilon}{k} - C_{\varepsilon_2} f_2 \frac{\varepsilon^2}{k} + \left(C_1 \nu \nu_t S^{*2}_{,j} + C_2 \nu \frac{k}{\varepsilon} k_{,j} S^* S^*_{,j}\right) f_{w_1} \tag{4}$$

$$-\overline{u_i u_j} = 2\nu_t S_{ij} - \tfrac{2}{3} k \delta_{ij} + C_{\alpha_1} \nu_t \frac{k}{\varepsilon}(S_{im} S_{mj} - \tfrac{1}{3} S_{mn} S_{mn} \delta_{ij}) + C_{\alpha_2} \nu_t \frac{k}{\varepsilon}(\omega_{im} S_{mj} + \omega_{jm} S_{mi}) + C_{\alpha_3} \nu_t \frac{k}{\varepsilon}(\omega_{im}\omega_{mj} - \tfrac{1}{3}\omega_{mn}\omega_{mn}\delta_{ij}) \tag{5}$$

$$\nu_t = C_\mu f_\mu \frac{k^2}{\varepsilon} \tag{6}$$

$$f_{\mu_1} = (1 - f_{w_1})(1 + 10 f_{w_1}/R_t^{1.25}) \tag{7}$$

$$f_{\mu_2} = C_{\mu_1} \frac{(C_{\mu_2} + C_{\mu_3} P_k/\varepsilon)}{(C_{\mu_2} + P_k/\varepsilon)^2}. \tag{8}$$

The unknown Reynolds stress $-\overline{u_i u_j}$ is expanded up to the second-order term in a nonlinear k–ε model [20, 21]. The nonequilibrium effect (P_k/ε) is incorporated into $C^*_{\varepsilon_1}$ which has the form $C^*_{\varepsilon_1} = C_{\varepsilon_1}$ $(0.95 + 0.05\ P_k/\varepsilon)$. S^* is a modified strain rate parameter, $S^* = 2.75\sqrt{\nu\varepsilon}/(\nu + \nu_t)$. The model constant C_1, C_2, C_{ε_1} and C_{ε_2} are set as $C_1 = 1.0$, $C_2 = 0.006$, $C_{\varepsilon_1} = 1.45$ and $C_{\varepsilon_2} = 1.9$, respectively. C_{α_1}, C_{α_2}, C_{α_3} and C_μ are the model constants ($C_{\alpha_1} = 0.6$, $C_{\alpha_2} = 0.4$, $C_{\alpha_3} = 0.005$ and $C_\mu = 0.09$). The damping function f_μ is expressed as $f_\mu = f_{\mu_1} f_{\mu_2}$, which reflects the effect of wall-proximity (f_{μ_1}) and of nonequilibrium on the effect of eddy viscosity away from the wall (f_{μ_2}).

3. TURBULENCE MODEL FOR THERMAL FIELD

3.1. *Governing equations*

The governing equations for turbulent heat transports are expressed as [17]

$$U_j \frac{\partial T}{\partial x_j} = \frac{\partial}{\partial x_j}\left[\alpha \frac{\partial T}{\partial x_j} - \overline{u_j \theta}\right] \tag{9}$$

$$-\overline{u_j \theta} = \alpha_t \frac{\partial T}{\partial x_j} \tag{10}$$

$$\alpha_t = C_\lambda f_\lambda \frac{k^2}{\varepsilon} \tag{11}$$

$$U_j \frac{\partial k_\theta}{\partial x_j} = \frac{\partial}{\partial x_j}\left[\left(\alpha + f_h \frac{\alpha_t}{\sigma_h}\right)\frac{\partial k_\theta}{\partial x_j}\right] + P_\theta - \varepsilon_\theta \tag{12}$$

$$U_j \frac{\partial \varepsilon_\theta}{\partial x_j} = \frac{\partial}{\partial x_j}\left[\left(\nu + f_h \frac{\alpha_t}{\sigma_\phi}\right)\frac{\partial \varepsilon_\theta}{\partial x_j}\right] - C_{P_1} \frac{\varepsilon_\theta}{k_\theta} \overline{u_j \theta} \frac{\partial T}{\partial x_j} - C_{P_2} \frac{\varepsilon_\theta}{k} \overline{u_i u_j} \frac{\partial U_i}{\partial x_j} - C_{D_1} f_{D_1} \frac{\varepsilon_\theta^2}{k_\theta} - C_{D_2} f_{D_2} \frac{\varepsilon \varepsilon_\theta}{k}. \tag{13}$$

As shown in the above, the eddy diffusivity for heat α_t in equation (11) is modeled in a manner similar to ν_t. Here, C_λ and f_λ are the model constant and the wall-damping function, respectively. The f_λ function is modeled to account for the effect of wall-proximity (f_{λ_1}) as well as the effect of nonequilibrium (f_{λ_2}). The detailed model formulations for f_λ and the ε_θ equation are elucidated in the following section, in conjunction with the temperature variance (k_θ) and its dissipation rate (ε_θ) together with k and ε.

3.2. *Formulations of* f_{λ_1} *and* f_{λ_2}

For the accurate prediction of heat transfer in separated and reattaching flows, it is highly important to reproduce the near-wall limiting behavior correctly. In the near-wall region, the asymptotic behaviors of instantaneous velocity and temperature maintain the relations $-\overline{v\theta} \propto y^3$, $\partial T/\partial y \propto y^0$, $\alpha_t \propto y^3$, $k \propto y^2$ and $\varepsilon = \nu\overline{(\partial u_i/\partial x_j)(\partial u_i/\partial x_j)} \to \varepsilon_w$ for $y \to 0$. Consequently, the damping function f_λ in equation (11) has to satisfy the relation, $f_\lambda \propto y^{-1}$. As is well known, the nonequilibrium effect becomes dominant in the region of separated and reattaching flows. In order to account for this effect in the present model, a decomposition of f_λ is attempted, i.e. $f_\lambda = f_{\lambda_1} f_{\lambda_2}$. The main rationale for this decomposition is that f_{λ_1} is intended to represent the damping effect near the wall and f_{λ_2} is considered for the nonequilibrium effect away from the wall.

In the first, the modeling of f_{λ_1} is taken into consideration. In a manner similar to the formulation of f_{μ_1} in flow fields, f_{λ_1} is expressed as

$$f_{\lambda_1} = (1 - T_{w_1})(1 + 10 T_{w_1}/R_t^{1.25}) \tag{14}$$

$$T_{w_1} = \exp\left[-\left(\frac{R_y}{80/\sqrt{Pr}}\right)^2\right], \tag{15}$$

where Pr denotes the Prandtl number. The wall-reflection function T_{w_1} represents the effect of wall-proximity in the near-wall region. As pointed out earlier, f_{λ_1} is found to satisfy the wall limiting behavior, i.e. $f_{\lambda_1} \propto y^{-1}$ [14].

Next, the effect of nonequilibrium away from the wall ($f_{\lambda_1} = 1$) is inspected. Since the modeling of turbulent heat transfer in separated and reattaching flows is dealt with in the present study, we should consider both the effect of nonequilibrium of the velocity field (P_k/ε) and that of the thermal field ($P_\theta/\varepsilon_\theta$). Here, P_θ represents the rate of production of the temperature fluctuations, $P_\theta \equiv -2\overline{u_i\theta}\partial T/\partial x_i$. In order to formulate the f_{λ_2} form in the nonequilibrium region, the concept of the algebraic stress/flux model is employed [22]:

$$\overline{u_i\theta} = \frac{2kk_\theta(P_{i\theta}+\phi_{i\theta})}{k_\theta(P_k-\varepsilon)+k(P_\theta-\varepsilon_\theta)}, \tag{16}$$

where $P_{i\theta}$ denotes the production rates of $\overline{u_iu_j}$ and $\overline{u_i\theta}$, respectively, i.e. $P_{i\theta} = -\overline{u_iu_j}\partial T/\partial x_j - \overline{u_j\theta}\partial U_i/\partial x_j$. $\phi_{i\theta}$ represents the pressure–temperature-gradient correlation, $\phi_{i\theta} = \overline{p\partial\theta/\partial x_i}$ [22].

In order to extract a relation f_{λ_2} from equation (16), some manipulations are needed. For example, for an attached boundary-layer flow, the following turbulent heat flux may be expressed as

$$\overline{v\theta} = \frac{2kk_\theta(P_{2\theta}+\phi_{2\theta})}{k_\theta(P_k-\varepsilon)+k(P_\theta-\varepsilon_\theta)}. \tag{17}$$

In the above, $P_{i\theta}$ becomes $P_{2\theta} = -\overline{v^2}\partial T/\partial y$, which is the term normal to the wall. In this form, the normal velocity fluctuation term has been already derived in the velocity field [1]:

$$\overline{v^2} = \tfrac{2}{3}k - \frac{2}{3}\frac{(1-C_2)P_k/\varepsilon}{P_k/\varepsilon+(C_1-1)}k. \tag{18}$$

The $\phi_{2\theta}$ term in equation (17) is modeled as [22]

$$\phi_{2\theta} = -C_{1\theta}\frac{\varepsilon}{k}\overline{v\theta}, \tag{19}$$

where $C_{1\theta}$ is the model constant ($C_{1\theta} = 3$). Substitution of equation (19) into equation (17) gives the following expression for $\overline{v\theta}$:

$$\begin{aligned} -\overline{v\theta} &= \frac{4(C_2P_k/\varepsilon+C_1-1)}{3\left\{2C_{1\theta}-1+P_k/\varepsilon+\dfrac{P_\theta/\varepsilon_\theta-1}{R}\right\}(P_k/\varepsilon+C_1-1)} \\ &\quad\times\frac{k^2}{\varepsilon}\frac{\partial T}{\partial y} \\ &= C_\lambda f_{\lambda_2}\frac{k^2}{\varepsilon}\frac{\partial T}{\partial y}, \end{aligned} \tag{20}$$

where the model function f_{λ_2} can be formulated, which accounts for the nonequilibrium effect away from the wall. As is evident, f_{λ_2} is a function of the parameters of nonequilibrium, i.e. P_k/ε and $P_\theta/\varepsilon_\theta$. A simplified f_{λ_2} is expressed as

$$f_{\lambda_2} = \frac{C_{\lambda_1}+C_{\lambda_2}P_k/\varepsilon}{(C_{\lambda_3}+P_k/\varepsilon)(C_{\lambda_4}+P_k/\varepsilon+(P_\theta/\varepsilon_\theta-1)/R)}, \tag{21}$$

where R is the ratio of the characteristic decay times for the turbulent temperature and velocity fields, $R \equiv (k_\theta/\varepsilon_\theta)/(k/\varepsilon)$. The new model constants are readjusted as $C_{\lambda_1} = 10.71$, $C_{\lambda_2} = 4.29$, $C_{\lambda_3} = 1.5$ and $C_{\lambda_4} = 5.0$, respectively.

On the other hand, it is important to note that the effect of nonequilibrium of the velocity field (P_k/ε) has been fully accounted for in the velocity model [1]. In order to avoid these duplicate considerations, a more simplified f_{λ_2} is proposed in the present study:

$$f_{\lambda_2} = \frac{6}{6+(P_\theta/\varepsilon_\theta-1)/R}. \tag{22}$$

As can be seen in equation (22), f_{λ_2} is formulated from equation (21) by setting $P_k/\varepsilon = 1$. The influence of the nonequilibrium ($P_k/\varepsilon \neq 1$) on f_{λ_2} has been scrutinized, however, the relatively small effects are estimated. Computations have been made for the flow behind a backward-facing step, and the results indicate that the f_{λ_2} form in equation (22) depicts the dominant heat transfer characteristics satisfactorily.

3.3. *Modeling of the ε_θ equation*

The ε_θ-equation can be modeled in a similar way to the prior models [14, 16, 17]:

$$\begin{aligned} U_j\frac{\partial\varepsilon_\theta}{\partial x_j} &= \frac{\partial}{\partial x_j}\left[\left(\nu+f_h\frac{\alpha_t}{\sigma_\phi}\right)\frac{\partial\varepsilon_\theta}{\partial x_j}\right]-C_{P_1}\frac{\varepsilon_\theta}{k_\theta}\overline{u_j\theta}\frac{\partial T}{\partial x_j} \\ &\quad -C_{P_2}\frac{\varepsilon_\theta}{k}\overline{u_iu_j}\frac{\partial U_i}{\partial x_j}-C_{D_1}f_{D_1}\frac{\varepsilon_\theta^2}{k_\theta}-C_{D_2}f_{D_2}\frac{\varepsilon\varepsilon_\theta}{k}. \end{aligned} \tag{23}$$

In the above equation, f_h is the model function for turbulent diffusion. It is revealed that the roles of turbulent diffusion are substantial in the near-wall region [1, 23]. In the present study, the following model is thus proposed as

$$f_h = 1+50\exp\left[-\frac{R_t}{150}\frac{R_t}{25/\sqrt{R\,Pr}}\right],$$

which is modified from the f_t function in the velocity fields [1]. The same model function f_h is used in the k_θ-equation. The model constants C_{P_1} and C_{P_2} for the production terms in the ε_θ-equation are determined by fitting the DNS data [18, 19], i.e. $C_{P_1} = 0.9$ and $C_{P_2} = 0.72$, respectively. These values are shown to be very close to those of other models [14, 16, 17].

The limiting behavior of wall turbulence should be taken into account to balance the ε_θ-budget in the near-wall region. It is known that the near-wall asymptotic behavior of wall turbulence is derived as: $k \sim y^2$ and $k_\theta \sim y^2$. Thus, the following relations are required to avoid the singularities of the ε_θ-equation near the wall, i.e. $f_{D_1} \propto y^2$ and $f_{D_2} \propto y^2$. Based on this reasoning, the damping function f_{D_1} is modeled $f_{D_1} = 1-\exp(-0.06R_y)$, which is basically the Van-Driest form. Note that R_y is also used instead of y^+ to cope with the difficulties in separated and reattaching flows.

In order to model the f_{D_2} function and determine the model constants (C_{D_1} and C_{D_2}), the decay law of homogeneous turbulence is employed in the present study [14]. In a homogeneous decaying turbulent flow, the ε_θ-equation becomes simply

$$U\frac{\partial \varepsilon_\theta}{\partial x} = -C_{D_1} f_{D_1} \frac{\varepsilon_\theta^2}{k_\theta} - C_{D_2} f_{D_2} \frac{\varepsilon \varepsilon_\theta}{k}, \quad (24)$$

where the x-axis is taken in the flow direction. By manipulating the other equations (k, ε and k_θ) for a homogeneous decaying turbulence, we also obtain

$$U\frac{\partial \varepsilon_\theta}{\partial x} = -\frac{\varepsilon_\theta^2}{k_\theta} - (C_{\varepsilon_2} f_2 - 1)\frac{\varepsilon \varepsilon_\theta}{k}. \quad (25)$$

Here, the function f_2 is modeled by considering the effect of free-turbulence [1].

Equations (24) and (25) yield the following relations $C_{D_1} f_{D_1} = 1$ and $C_{D_2} f_{D_2} = C_{\varepsilon_2} f_2 - 1$. If we suppose the initial period of decaying turbulence ($f_{D_1} = f_{D_2} = f_2 = 1$), the model constants can be set as $C_{D_1} = 1$ and $C_{D_2} = 0.9$ [14]. Next, the f_{D_2} model function can be modeled as

$$f_{D_2} = \frac{C_{\varepsilon_2} f_2 - 1}{C_{D_2}} f_{D_w},$$

where the leading term, i.e. $(C_{\varepsilon_2} f_2 - 1)/C_{D_2}$ represents the effect of free-turbulence and f_{D_w} denotes the wall-proximity near the wall. f_{D_w} is obtained by fitting the DNS data

$$f_{D_w} = 1 - \exp(-0.06R_y)[\cos(0.88\sqrt{R_y}) + 0.493\sqrt{R_y}\sin(0.88\sqrt{R_y})].$$

The use of f_{D_w} reveals that the near-wall behaviors in separated and reattaching flows can be resolved with a good accuracy. Obviously, f_{D_2} satisfies the limiting behavior $f_{D_2} \propto y^2$.

4. RESULTS AND DISCUSSION

The main aim of the present model is to predict turbulent thermal quantities in separated and reattaching flows. However, it is important to ascertain the generality and accuracy of the present model to an attached boundary layer. Since the turbulence quantities are quantitatively available from DNS data [18, 19], first we have applied the model to a fully developed channel flow with two typical boundary conditions, i.e. with a uniform wall temperature and a uniform heat flux. Next, the proposed model is tested for the combined heat and fluid flow over a backward-facing flow and the flow over a blunt flat plate. These flow configurations are frequently used for benchmarking the performance of turbulence models for separated and reattaching flows. The model predictions are compared with the experimental data of Vogel and Eaton [5] for a backward-facing step flow and Ota and Kon [6] for a flow over a blunt flat plate.

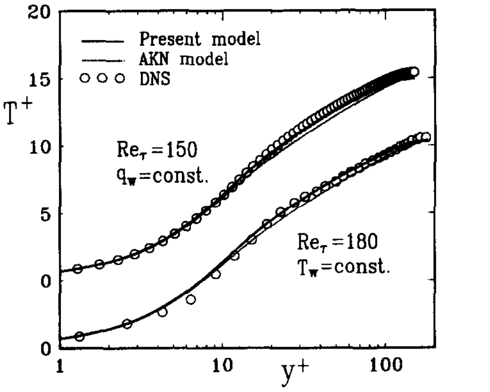

Fig. 1. Comparison of the predicted T with the DNS data.

4.1. *Model performance in an attached boundary layer*

The numerical scheme used is a well-established finite-volume method. The boundary conditions are:

$$U = k = k_\theta = 0, \quad \varepsilon = \nu\partial^2 k/\partial y^2, \quad \varepsilon_\theta = \alpha\partial^2 k_\theta/\partial y^2,$$

$$T_w = \textit{constant} \text{ or } q_w = \textit{constant} \text{ at the wall;}$$

$$\partial U/\partial y = \partial k/\partial y = \partial \varepsilon/\partial y = \partial T/\partial y = \partial k_\theta/\partial y = \partial \varepsilon_\theta/\partial y = 0$$

at the central axis. In order to obtain the grid-independent solutions, we need 101 nonuniform grid points in the direction normal to the wall. The grid convergence was checked and the outcome of these tests were found to be satisfactory.

The predicted profiles of temperature T^+ by the present model are exhibited in Fig. 1 under two different wall thermal conditions. The selected Reynolds numbers are $Re_\tau = 150$ and 180, for which the DNS data exist. The model predictions by Abe *et al.* [17] (hereafter referred to as AKN model) are also displayed for comparisons. This is based on the belief that the AKN model is recently developed and can be regarded as a reliable model for predicting fluid flow and heat transfer in separated and reattaching flows. As seen in Fig. 1, the present model shows good predictions with the DNS data for both the uniform wall temperature and uniform wall heat flux conditions [18, 19], while the AKN model slightly underpredicts in the outer region of a boundary layer ($y^+ > 50$).

The predicted profiles of temperature variance k_θ^+ are shown in Fig. 2. The DNS data of Kim and Moin [18], with a uniform wall temperature condition ($T_w = \textit{constant}$), is included for comparison. Both the present model and the AKN model provide predictions similar to the DNS data, however, the predicted results are slightly underpredicted. Compared to the prior k^+ profile in velocity fields by Park and Sung [1], the predicted k_θ^+ profile is seen to be less accurate. The near-wall behavior of ε_θ^+ is shown in Fig. 3. The DNS data of Kasagi *et al.* [19] is employed with the uniform wall heat flux condition, i.e. $q_w = \textit{constant}$. As shown in Fig. 3, the present model gives good agreement with the DNS data. In particu-

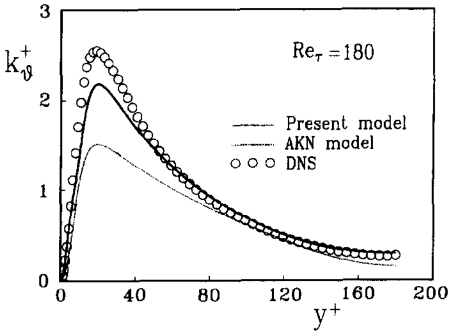

Fig. 2. Comparison of the predicted k_θ with the DNS data.

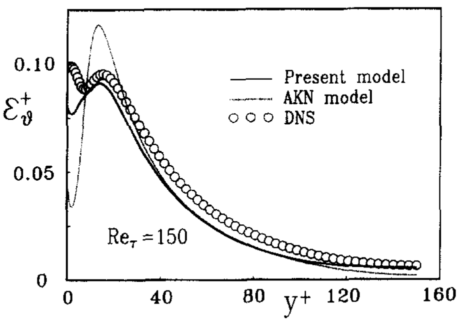

Fig. 3. Comparison of the predicted ε_θ with the DNS data.

lar, the present model follows the wall behavior fairly well. As pointed out in the f_{λ_1} formulation, the turbulent heat flux $\overline{v\theta}$ needs to satisfy the near-wall asymptotic behavior of $\overline{v\theta} \propto y^3$. It is found that this relation is reproduced accurately in the near-wall region.

4.2. *Model performance in separated and reattaching flows*

As mentioned earlier, two benchmarking experimental results are selected to test the model for separated and reattaching flows; a backward-facing step flow [5] and a flow over a blunt flat plate [6]. Before proceeding further, the boundary conditions and numerical procedure for these elliptic computations are briefly summarized in the following. The boundary conditions are: $U = V = k = k_\theta = 0$, $\varepsilon = \nu\partial^2 k/\partial n^2$, $\varepsilon_\theta = \alpha\partial^2 k_\theta/\partial n^2$, $\partial P/\partial n = 0$ and $q_w = constant$ at the bottom wall surface. The inlet conditions are given from the experimental conditions together with $\partial P/\partial n = 0$. Table 1 lists the experimental conditions

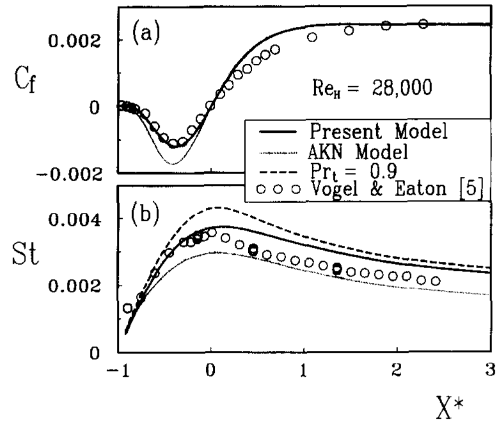

Fig. 4. (a) Comparison of the predicted C_f with the experimental data, (b) comparison of the predicted St with the experimental data.

for two cases [5, 6]. The Neuman conditions are applied at the outlet. The specifics regarding the numerical procedure and grid resolution are found in Park and Sung [1].

As a validation of flow field computation, the wall shear stress coefficient (C_f) is exhibited in Fig. 4(a), which is closely related to the prediction of turbulent heat transfer near the wall. The predicted (C_f) is plotted against a nondimensional streamwise coordinate $X^* = (X - X_R)/X_R$, together with the experimental data of Vogel and Eaton [5]. Here, X_R represents the reattachment length. The step-height Reynolds number is $Re_H = 28\,000$. It is seen that the present model prediction in the recirculation region is in better agreement with the experiment than the AKN model prediction.

The Stanton number St profiles are displayed in Fig. 4(b) by using the same coordinate X^*. The Stanton number profiles by employing the turbulent Prandtl number $Pr_t = 0.9$, without solving the k_θ, ε_θ equations, are also plotted in Fig. 4(b). The comparison between the predicted results and the experimental data indicates that the present model prediction is in overall better agreement with the experiment. The predicted result of $Pr_t = 0.9$ is overpredicted near the recirculation region. However, all of the Stanton number profiles have the same general features, i.e. the peak heat transfer rates occurs near the reattachment region ($X^* = 0$) and there is a low heat transfer rate in the

Table 1. Experimental conditions

Vogel and Eaton [5] flow over a backward-facing step		Ota and Kon [6] flow over a blunt flat plate	
Reynolds number	$Re_H = 28\,000$	Reynolds number	$Re_H = 12\,000$
Expansion ratio	$ER = 1.25$	Half plate thickness	$H = 0.011$ m
Inlet conditions	$Re_\theta = 3370$	Inlet conditions	$U_\infty = 18.8$ m s^{-1}
	$\delta/H = 1.1$		$\sqrt{\overline{u^2}}/U_\infty \leq 0.8\%$
Heat flux at wall	270 W m^{-2}	Heat flux at wall	1.7 kW m^{-2}
Grid mesh	201×101	Grid mesh	201×101

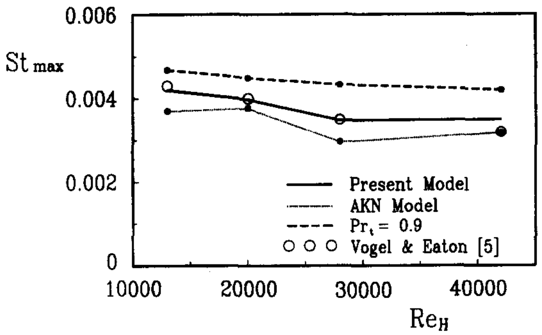

Fig. 5. Comparison of the predicted St_{max} with the experimental data.

recirculation region. The heat transfer coefficient recovers fairly rapidly to flat-plate behavior downstream of reattachment [5].

Comparisons are extended to the maximum Stanton number St_{max} in Fig. 5. The maximum Stanton number for $\delta/H = 1.1$ is plotted by varying Re_H ($13\,000 \leqslant Re_H \leqslant 42\,000$). Here, δ/H represents the initial boundary layer thickness normalized by the step height H. It is clearly seen that the present computed results are in excellent agreement with the experiment. However, the predicted results by assuming $Pr_t = 0.9$ are seen to be slightly overpredicted, while the AKN model underpredicts. In general, it is known that St_{max} is a function of Re_H [5]. In Fig. 5, St_{max} is shown to be monotonically decreased as Re_H increases.

The profiles of turbulent flux $(\overline{v\theta}^+)$ near the recirculation region ($-0.7 \leqslant X^* \leqslant 0.5$) are shown in Fig. 6. The step height Reynolds number is $Re_H = 13\,000$ and $\delta/H = 1.1$, respectively. As can be seen, rather poor agreement is obtained between the predicted results and the experiment [5]. Moreover, the deviation is amplified near the wall region. This inadequate prediction may be attributable to the fact of incompleteness of the present model. On the other hand, as stressed by Vogel and Eaton [5], the fall off of the turbulent transport approaching the wall may

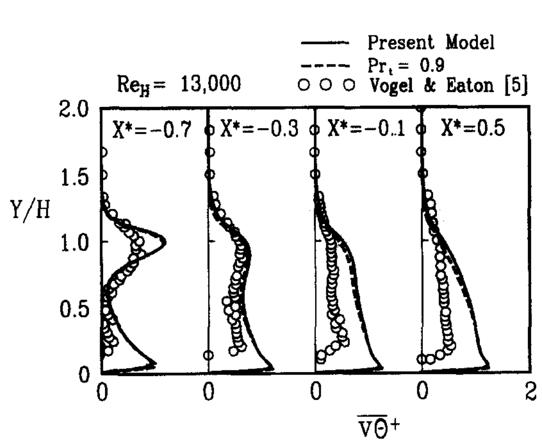

Fig. 6. Comparison of the predicted $-\overline{v\theta}$ with the experimental data.

be exaggerated due to the constraint of their measurement technique. However, the overall trends between them are generally consistent. It is seen that the change near the step is representative of the shift in the turbulent transport between a free shear layer and a wall-boundary flow. At the position downstream of one half reattachment ($X^* = 0.5$), the profile is very similar to that found on a flat plate, i.e. $\overline{u\theta}^+$ highest near the wall, dropping to zero in the free stream.

Based on the wealth of numerical results, it is useful to visualize the contour plots of $Pr_t(=\alpha_t/\nu_t)$. The iso-contour lines of Pr_t are plotted in Fig. 7. It should be noted that the direct measurement of Pr_t is very cumbersome. However, it is true that the Pr_t distributions for turbulent separated and reattaching flows are informative for understanding the heat transport characteristics. As shown in Fig. 7, the assumption of $Pr_t = constant$ is admittable to some extent in the region of no recirculations. However, a closer inspection of the enlarged view near the recirculating region discloses that the assumption of $Pr_t = constant$ is not acceptable. Near the separation point, it is found that Pr_t increases considerably. This may be attributed to the fact that an active heat transfer exists between the cold approaching stream and the hot recirculating thermal plume from the heated wall, i.e. α_t is enhanced. Furthermore, Pr_t increases in the separated free-shear layer. On the contrary, relatively small values of ν_t and α_t are obtained in the present computation very close to the wall.

Further evidence of the present model performance is seen in the plot of the time scale ratio $R = (k_\theta/\varepsilon_\theta)/(k/\varepsilon)$ in Fig. 8. The time scale ratio is defined by the ratio of the time scale of energy containing eddies in the thermal field $(k_\theta/\varepsilon_\theta)$ to that in a velocity field (k/ε). Since the turbulent mixing in the separated free-shear layer is so strong, the velocity time scale (k/ε) becomes very small. In contrast, the thermal time scale $(k_\theta/\varepsilon_\theta)$ is relatively large from the computation. This shows that R is very large along the separated free-shear layer.

Finally, the flow over a flat plate with blunt leading-edge is calculated by the present model. Comparisons are made with the experimental data [6]. The relevant experimental conditions are listed in Table 1. The distributions of the turbulent heat flux at several cross-sections, including the separated, reattached and redeveloped flow regions, are shown in Fig. 9. It is seen that the present model predictions are in broad agreement with the experiment. However, relatively large deviations are displayed around the reattachment point. These discrepancies may be attributed to their experimental procedure. As stated by Ota and Kon [6], the turbulent heat flux was estimated from Kramer's formula. This formula is based on the assumption that the turbulent fluctuating velocity and temperature are very small, as compared with the corresponding mean values. It means that the turbulent shear stress may not be affected by heating the wall. They addressed that the experimental uncertainty may be of an order

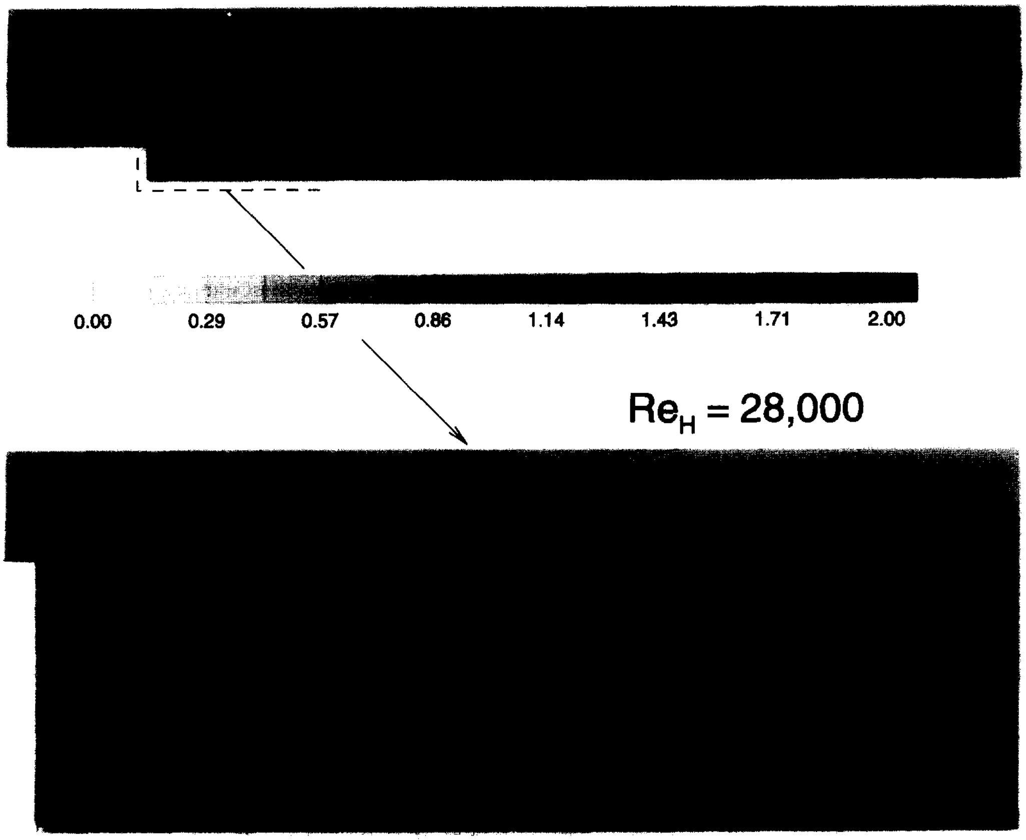

Fig. 7. Contour plots of Pr_t in a backward-facing step flow.

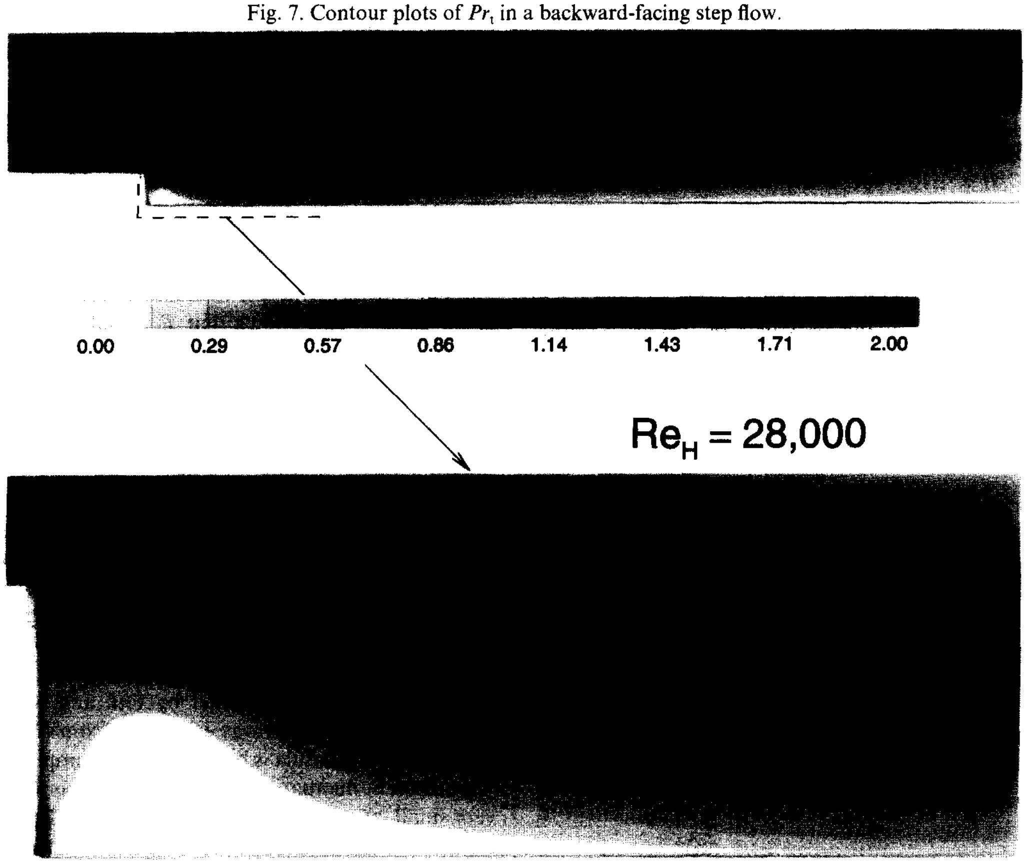

Fig. 8. Contour plots of R in a backward-facing step flow.

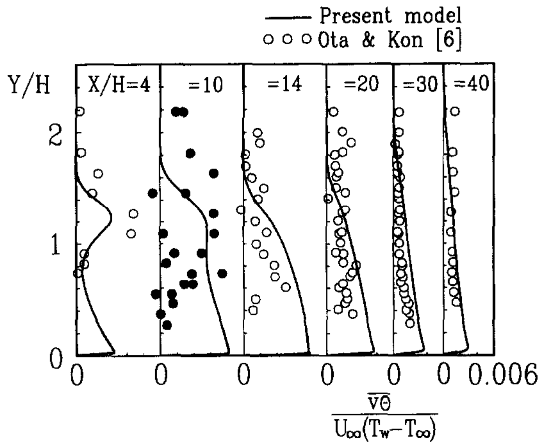

Fig. 9. Comparison of the predicted $-\overline{v\theta}$ with the experimental data.

of $\pm 50\%$ in the reattaching flow region. However, in the redeveloping region, the agreement between computation and experiment is seen to be satisfactory.

5. CONCLUSION

An improved version of the low-Reynolds-number k_θ–ε_θ model has been developed for predicting heat transfer in turbulent separated and reattaching flows. Emphasis was placed on the adoption of $R_y(\equiv k^{1/2}y/\nu)$ instead of $y^+(\equiv u_\tau y/\nu)$ in the low-Reynolds-number model. The limiting near-wall behavior close to the wall and the nonequilibrium effect in the recirculating region away from the wall were fully taken into consideration. The wall limiting behavior of the ε_θ-equation was also incorporated. In the first, the present model was tested against the DNS data of a fully developed channel flow with a uniform wall temperature and with a uniform heat flux. The near-wall behaviors of k_θ and ε_θ were reproduced fairly well. Next, the validation was extended to the flow over a backward-facing step and the flow over a blunt flat plate. In testing the backward-facing step flow, the predicted results of wall shear stress coefficient (C_f) and Stanton number (St) were shown to be in good agreement with the relevant experiment. In particular, the maximum Stanton number (St_{max}) showed excellent agreement with the experiment. It was revealed that the present model prediction is in overall better agreement with the experiment than the case of $Pr_t = 0.9$. Relatively poor agreement was obtained for the predictions of turbulent heat flux. However, the overall trends were generally satisfactory. From the contour plots of Pr_t and R, valuable information could be extracted. For the prediction of turbulent heat transfer over a blunt flat plate, the profiles of turbulent heat flux were calculated and compared with the experiment. They were found to be qualitatively consistent with the experiment.

REFERENCES

1. T. S. Park and H. J. Sung, A nonlinear low-Reynolds-number k–ε model for turbulent separated and reattaching flows—I. Flow field computations, *Int. J. Heat Mass Transfer* **38**, 2657–2666 (1995).
2. L. S. Fletcher, D. G. Briggs and R. H. Page, Heat transfer in separated and reattaching flows: an annotated review *Israel J. Tech.* **12**, 236–261 (1974).
3. W. Aung and C. B. Watkins, Heat transfer mechanisms in separated forced convection, *Proceeding of the NATO Institute on Turbulent forced Convection in Channels and Bundles: Theory and Applications to Heat Exchangers*, Turkey (1978).
4. W. Aung and R. J. Goldstein, Heat transfer in separated flow downstream of a rearward-facing step, *Israel J. Tech.* **10**, 35–44 (1972).
5. J. C. Vogel and J. K. Eaton, Combined heat transfer and fluid dynamic measurements downstream of a backward-facing step, *Trans. ASME J. Heat Transfer* **107**, 922–929 (1985).
6. T. Ota and N. Kon, Turbulent transfer of momentum and heat in the separated and reattached flow over a blunt flat plate, *Trans. ASME J. Heat Transfer* **102**, 749–754 (1980).
7. M. Ciofalo and M. W. Collins, k–ε predictions of heat transfer in turbulent recirculating flows using an improved wall treatment, *Numer. Heat Transfer B* **15**, 21–47 (1989).
8. C. C. Chieng and B. E. Launder, On the calculation of turbulent heat transport downstream from an abrupt pipe expansion, *Numer. Heat Transfer* **3**, 189–207 (1980).
9. S. Dutta and S. Acharya, Heat transfer and flow past a backstep with the nonlinear k–ε turbulence model and the modified k–ε turbulence model, *Numer. Heat Transfer A* **23**, 281–301 (1993).
10. B. Arman and T. J. Rabas, Two-layer-model predictions of heat transfer inside enhanced tubes, *Numer. Heat Transfer A* **25**, 721–741 (1994).
11. S. B. Pope, Consistent modeling of scalars in turbulent flows, *Phys. Fluids* **26**, 404–408 (1983).
12. A. J. Reynolds, The prediction of turbulent Prandtl and Schmidt numbers, *Int. J. Heat Mass Transfer* **18**, 1055–1069 (1975).
13. R. A. Antonia, Behavior of the turbulent Prandtl number near the wall, *Int. J. Heat Mass Transfer* **23**, 906–908 (1980).
14. Y. Nagano and C. Kim, A two-equation model for heat transport in wall turbulent shear flows, *Trans. ASME J. Heat Mass Transfer* **110**, 583–589 (1988).
15. M. K. Chung and H. J. Sung, Four-equation turbulence model for prediction of the turbulence boundary layer affected by buoyancy force over a flat plate, *Int. J. Heat Mass Transfer* **27**, 2387–2395 (1984).
16. M. S. Youssef, Y. Nagano and M. Tagawa, A two-equation heat transfer model for predicting turbulent thermal fields under arbitrary wall thermal conditions, *Int. J. Heat Mass Transfer* **35**, 3095–3140 (1992).
17. K. Abe, T. Kondoh and Y. Nagano, A new turbulence model for predicting fluid flow and heat transfer in separating and reattaching flows—II. Thermal field calculations, *Int. J. Heat Mass Transfer* **38**, 1467–1481 (1995).
18. J. Kim and P. Moin, Transport of passive scalars in a turbulent channel flow, *Proceedings of the Sixth Symposium on Turbulent Shear Flows*, pp. 5.2.1–5.2.6 (1987).
19. N. Kasagi, Y. Tomita and A. Kuroda, Direct numerical simulation of passive scalar field in a turbulent channel flow, *Trans. ASME J. Transfer* **14**, 598–606 (1992).
20. R. Rubinstein and J. M. Barton, Nonlinear Reynolds

stress models and the renormalization group, *Phys. Fluids A* **2**, 1472–1476 (1990).
21. C. G. Speziale, Analytical methods for the development of Reynolds-stress closures in turbulence, *Ann. Rev. Fluid Mech.* **23**, 107–157 (1991).
22. M. M. Gibson and B. E. Launder, Ground effects on pressure fluctuations in the atmospheric boundary layer, *J. Fluid Mech.* **86**, 491–511 (1978).
23. N. Nagano and M. Shimada, Modeling the dissipation-rate equation for two-equation turbulence model, *Proceedings of the Ninth Symposium on Turbulent Shear Flows*, pp. 23.2.1–23.2.6 (1993).